Cell Reports
Physical Science

CellPress
OPEN ACCESS

Article

Fast detection and 3D imaging of nanoplastics and microplastics by stimulated Raman scattering microscopy

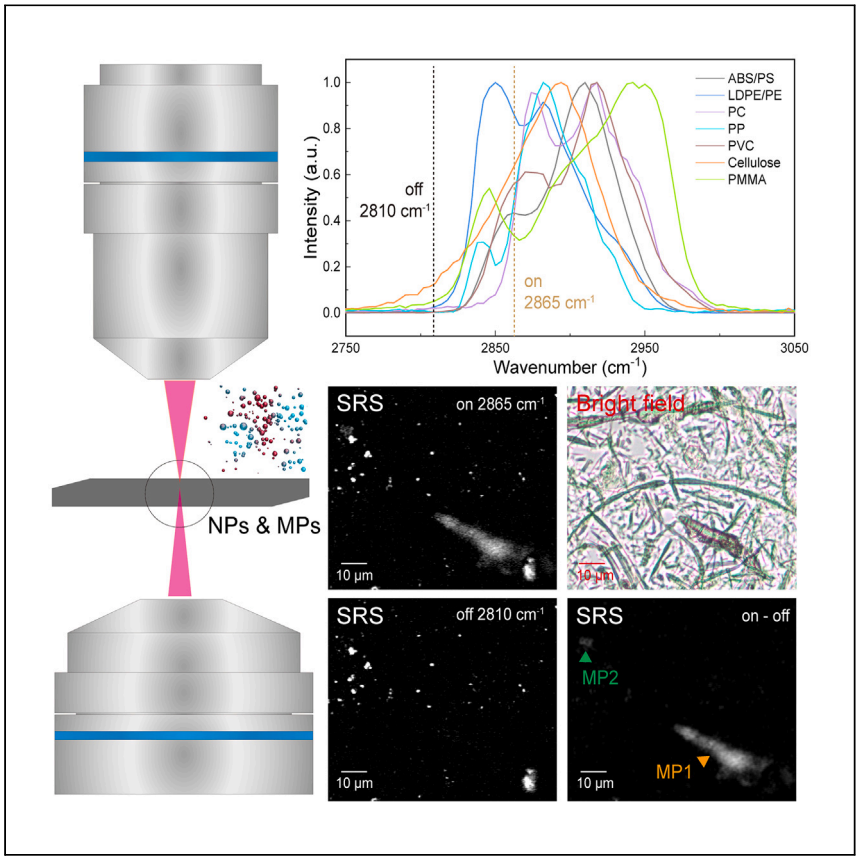

Ao et al. propose a 3D single-particle detection method based on stimulated Raman scattering microscopy for imaging nano- and microplastics. Two case studies demonstrate the real-world utility of this methodology, indicating promise for advancing characterization of plastics in both environmental and human tissue samples.

Jianpeng Ao, Guanjun Xu, Han Wu, ..., Tianxiang Chen, Minbiao Ji, Liwu Zhang

txchen@shsmu.edu.cn (T.C.)
minbiaoj@fudan.edu.cn (M.J.)
zhanglw@fudan.edu.cn (L.Z.)

Highlights

Stimulated Raman scattering microscopy enables 3D imaging at single-particle level

Nano-/microplastics can be distinguished with C-H stretching and fingerprint bands

Detection is demonstrated in atmospheric samples and human lung tissue samples

Ao et al., Cell Reports Physical Science 4, 101623
October 18, 2023 © 2023 The Authors.
https://doi.org/10.1016/j.xcrp.2023.101623

Please cite this article in press as: Ao et al., Fast detection and 3D imaging of nanoplastics and microplastics by stimulated Raman scattering microscopy, Cell Reports Physical Science (2023), https://doi.org/10.1016/j.xcrp.2023.101623

Cell Reports
Physical Science

Article

Fast detection and 3D imaging of nanoplastics and microplastics by stimulated Raman scattering microscopy

Jianpeng Ao,[2,5] Guanjun Xu,[1,5] Han Wu,[4,5] Lifang Xie,[1,5] Juan Liu,[1] Kedong Gong,[1] Xuejun Ruan,[1] Jin Han,[1] Kejian Li,[1] Wei Wang,[1] Tianxiang Chen,[4,*] Minbiao Ji,[2,*] and Liwu Zhang[1,3,6,*]

SUMMARY

Nanoplastic pollution represents an increasing concern for the scientific community. However, the identification of tiny nano-/microplastics (smaller than 5 μm) is still a huge challenge. Herein, we report rapid detecting and 3D imaging of nano-/microplastics at the single-particle level via a strategy based on stimulated Raman scattering microscopy. We demonstrate detection of nanoplastics as small as 100 nm and discriminate between different types of nanoplastics using high wavenumber scanning with low wavenumber verification. Nano-/microplastics, such as polyethylene and polypropylene, are detected in atmospheric and human lung tissue samples. This work provides a 3D, single-particle-level nano-/microplastics detection method, holding great potential to facilitate the characterization of nano-/microplastics in the environment and human tissues. By demonstrating the real-world utility of our methodology, we hope to foster wider adoption and understanding of this critical tool.

INTRODUCTION

Recently, the issue of microplastics has aroused widespread concern. Microplastics have the characteristics of small size (<5 mm), strong hydrophobicity, low density, and large specific surface area and can stay in the environment for a long time.[1,2] Furthermore, bulk microplastics can decay through mechanical abrasion, photodegradation, and biodegradation, forming nanoplastics (<1 μm), which are distinct from microplastics and have unique characteristics compared with engineered nanomaterials.[3] These nanoplastics have significantly more potent toxicological properties[4,5] due to the higher surface area-to-volume ratios that make them prone to sorb and release chemicals. Besides, their nanoscale size allows them to enter animal/plant cells and cross epithelial tissues more easily; if inhaled, airborne nanoplastics can even cross the pulmonary epithelial lining,[6,7] inducing a potential impact on biological organisms and even the entire ecosystem.

Microplastics and nanoplastics have been detected in many foods and daily necessities related to the human body. Research has shown that microplastics and nanoplastics were released from infant feeding bottles brewing in hot water, with particle numbers as high as 162,000,000 particles per liter.[8] Plastic teabags were reported to release millions of microparticles and nanoparticles during a typical steeping process,[9] while there are still debates about whether these particles are truly plastics.[10,11] In addition, polystyrene (PS) nanoplastics are detected in three aquatic animals that have a broad distribution in the benthic area, indicating that there is a

[1]Shanghai Key Laboratory of Atmospheric Particle Pollution and Prevention, Department of Environmental Science and Engineering, Fudan University, Shanghai 200433, People's Republic of China

[2]State Key Laboratory of Surface Physics and Department of Physics, Human Phenome Institute, Multiscale Research Institute of Complex Systems, Academy for Engineering and Technology, Key Laboratory of Micro and Nano Photonic Structures (Ministry of Education), Fudan University, Shanghai 200433, People's Republic of China

[3]Shanghai Institute of Pollution Control and Ecological Security, Shanghai 200092, People's Republic of China

[4]Shanghai Lung Cancer Center, Shanghai Chest Hospital, Shanghai Jiao Tong University School of Medicine, Shanghai 201109, People's Republic of China

[5]These authors contributed equally

[6]Lead contact

*Correspondence: txchen@shsmu.edu.cn (T.C.), minbiaoj@fudan.edu.cn (M.J.), zhanglw@fudan.edu.cn (L.Z.)

https://doi.org/10.1016/j.xcrp.2023.101623

potential exposure risk of humans to nanoplastics through the food chains.[12] Table salt, drinking water, and air are also ways of exposure to microplastics. Moreover, the intake of microplastics via inhalation is much higher than those via other ways.[13] Currently, stained polypropylene, a thermoplastic polymer, and other unknown microplastics are found in human placenta.[14] Besides, various microplastics were detected in all the experimental human stool samples,[15] suggesting inadvertent ingestion from different sources.

However, the current detection methods for microplastics, especially nanoplastics, are still limited. Electron microscopy,[16,17] Fourier infrared spectroscopy,[18,19] Raman spectroscopies,[20,21] pyrolysis-gas chromatography-mass spectrometry (Py-GC-MS),[12] and acid depolymerization-liquid chromatography-tandem MS (LC-MS/MS)[22] are methods applied to microplastics and nanoplastics detection and identification. Among them, Fourier infrared spectroscopy is limited by low spatial resolution, so it is more suitable for detecting particles above 20 μm and is difficult to use for small-size particles. Although traditional spontaneous Raman spectroscopy could reach ~500 nm resolution, the intrinsically weak Raman cross-sections require long integration times for signal acquisition, hindering its actual detection efficiency. Surface-enhanced Raman scattering (SERS) boosted Raman signals with designed enhancing substrates and has been applied to detect nanoplastics in the atmosphere, as reported in our previous work.[23] Nonetheless, the size for identification is limited to several hundred nanometers, and it suffers from uneven hotspots in the SERS substrate, which hinders its application in complex environmental samples. The detection of nanoplastics is still facing many challenges up to now. In quantitative analysis, accuracy and detection speed are still restrictive factors. Besides, 3D imaging analysis plays an important role in traceability analysis and morphological research, while the morphological characterization of microplastics in previous studies is limited by the constraints of tools and instruments, and it is difficult to achieve a balance between achieving high spatial resolution and obtaining comprehensive morphological features. Up to now, there has been no method or technology that could provide accurate 3D information of microplastic samples. At present, the research on nanoplastics is still in its infancy, and a technical means that can quickly and intuitively provide properties and 3D information of nanoplastics is urgently needed.

Stimulated Raman scattering (SRS) microscopy is an emerging technology that amplifies the Raman signal by a coherent non-linear optical process, enabling high-speed, 3D imaging with high chemical specificity and sensitivity to overcome such limitations.[24–27] Over the past decade, SRS microscopy has been rapidly developed and widely applied in many branches of biological and biomedical researches, such as label-free tumor histology, lipid metabolism, drug delivery, etc.[28,29] More recently, SRS has demonstrated advantages for studying materials science, exploiting its quantitative chemical imaging capability.[30–35] As plastics are a type of polymer material, each plastic variant exhibits unique Raman spectral features, making specific identification possible through SRS microscopy.[36] Therefore, the high spatial-temporal-chemical resolution of SRS microscopy is expected to provide a suitable tool for micro- and nanoplastics detection. The potential of SRS for rapid analysis of microplastics has garnered attention in the research community. Liao et al.[37] combined real-time SRS Raman analysis and imaging techniques to analyze PS and polymethyl methacrylate (PMMA) microbeads, and Zhang et al.[38] demonstrated the capability of SRS combined with flow cytometry for fast identification of plastic microspheres. In applications involving real environmental samples, SRS microscopy has been employed to swiftly identify various microplastic particles in estuarine sediments[39] and to determine the composition of environmental fibers

in surface seawater, coastal sediments, and deep-sea sediments.[40,41] However, existing SRS-based approaches for environmental sample analysis primarily focus on identifying polymer categories, primarily targeting larger microplastic particles (typically larger than 50 μm). This limitation results in an underestimation of the presence of submicron- and nanoplastics in environmental samples.

In this work, we demonstrated a strategy based on SRS for the rapid and accurate detection of micro- and nanoplastics. First, we achieved the determination of nano-/microplastics with sizes down to 100 nm and resolved different types of plastics in the mixture within the same field of view (FOV) at a wavenumber region between 2,750 and 3,050 cm^{-1}. Secondly, the high sensitivity of SRS enables the high-throughput quantitative study and 3D imaging of individual nanoplastic particles. Furthermore, micro-/nanoplastics in actual atmospheric samples and human lung tissues were successfully detected and characterized, demonstrating the potential practical studies for environmental science and human health.

RESULTS

Detection of nanoplastics with different sizes

As detailed in the supplemental experimental procedures, each SRS image taken by our setup depicts the spatial distribution of a specific Raman-active molecular vibration (Ω) in the sample (Figure 1A). To fulfill the purpose of detecting nano-/microplastics, the first key step is to determine the SRS imaging band. Micro-Raman spectroscopy (MRS) was used to test the PS microsphere, and its Raman spectrum was obtained as benchmark, as shown in Figure 1B. According to the spontaneous Raman spectrum, peaks at 1,000 and 1,029 cm^{-1}, originated from the breathing vibration and the symmetrical stretching vibration between carbon atoms in the benzene ring, present the strongest signals within the fingerprint region and could be set as characteristic peaks with high specificity. The corresponding SRS spectrum was taken when the pump-beam wavenumber was set as 942 nm. Meanwhile, we noticed that as the pump-beam wavenumbers changed to 790 and 801 nm, the resonance SRS images that matched with 3,050 and 2,910 cm^{-1} became brighter, as commonly seen in SRS where the high-frequency CH stretch signal has higher detection efficiency and the spectral possess characteristic line shapes. Therefore, all three bands (950–1,050, 2,800–2,950, and 3,000–3,100 cm^{-1}) were selected to represent PS in our SRS experiments, of which the wavenumbers of the corresponding pump beams were 942, 801, and 790 nm (Figure 1C), respectively. We performed hyper-spectral scanning to determine the type of plastics according to the spectral shape and peak positions (Figure S1). For the imaging of a standard PS microsphere, 790 nm was preferred because of the strongest SRS signal. PS microspheres, with gradually reduced particle sizes from 5 μm, 2 μm, 1 μm, 500 nm, and 360 nm, can be successfully detected at the single-particle level via SRS imaging, as shown in Figure 1D. We noticed that 100 nm PS nanospheres in SRS imaging were profiled as ∼360 nm rather than the actual size due to the optical diffraction limit, which could be further improved by doubling the frequency of excitation beams to the visible range and adapting an optimized objective with a higher numerical aperture (NA).[42] Nonetheless, as evidenced by scanning electron microscopy (SEM), the current imaging results already show that SRS can detect single 100 nm PS particles (Figure S2), which is far beyond the detection limit of spontaneous Raman single-point tests and mapping with or without enhancement.

In order to verify the chemical specificity of SRS in discriminating different types of nano-/microplastics, samples mixed with 2 μm and 500 nm PS, 5 and 2 μm PMMA,

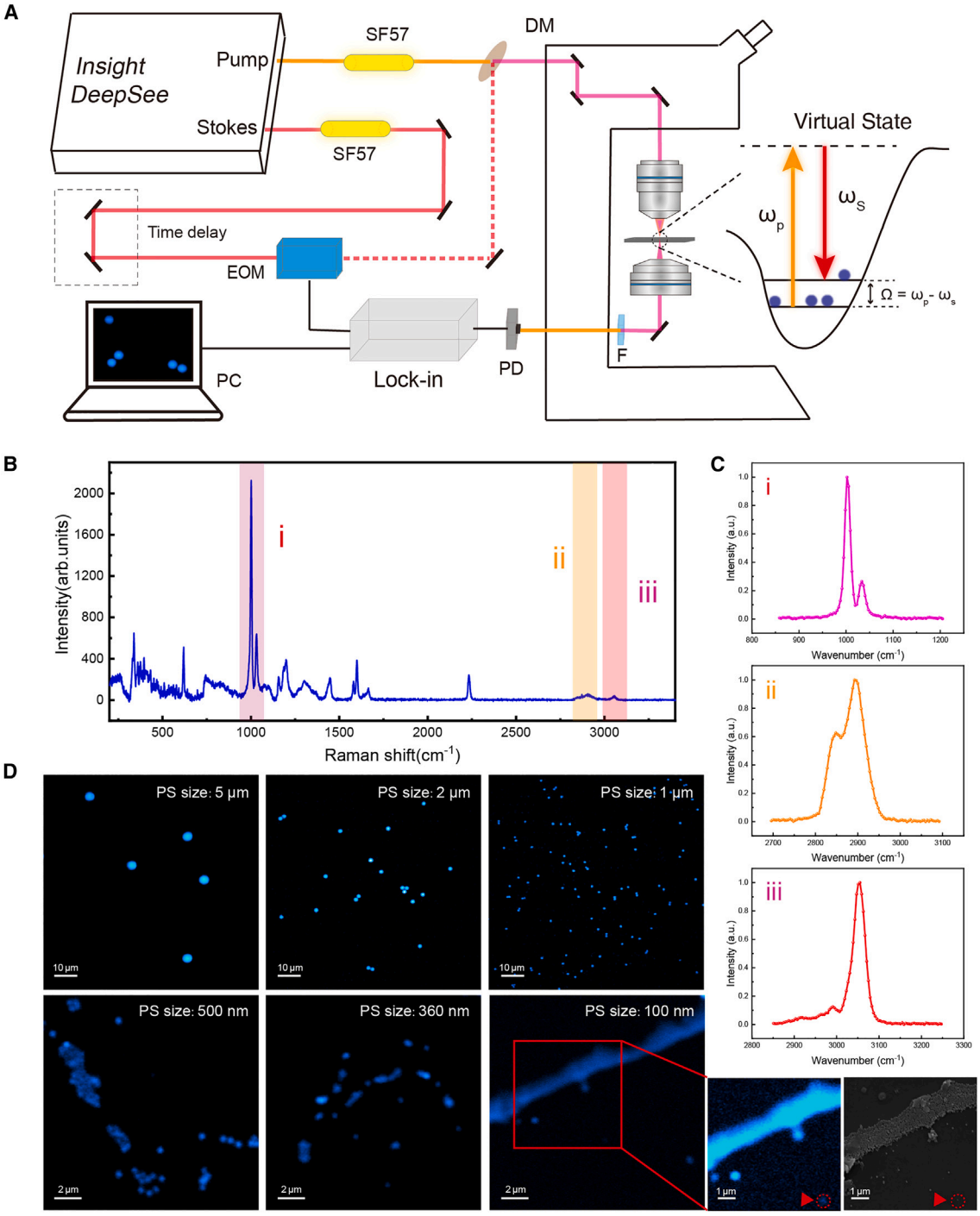

Figure 1. Detection of PS nano-/microplastics with different sizes via SRS

(A) Schematic illustration of SRS microscopy system.

(B) A typical MRS spectrum of PS.

(C) SRS spectra of PS.

(D) SRS imaging of PS with sizes of 5 μm, 2 μm, 1 μm, 500 nm, 360 nm, and 100 nm, respectively.

Scale bars: 10 μm (top), 2 μm (bottom), and 1 μm (zoomed-in image) in (D).

Please cite this article in press as: Ao et al., Fast detection and 3D imaging of nanoplastics and microplastics by stimulated Raman scattering microscopy, Cell Reports Physical Science (2023), https://doi.org/10.1016/j.xcrp.2023.101623

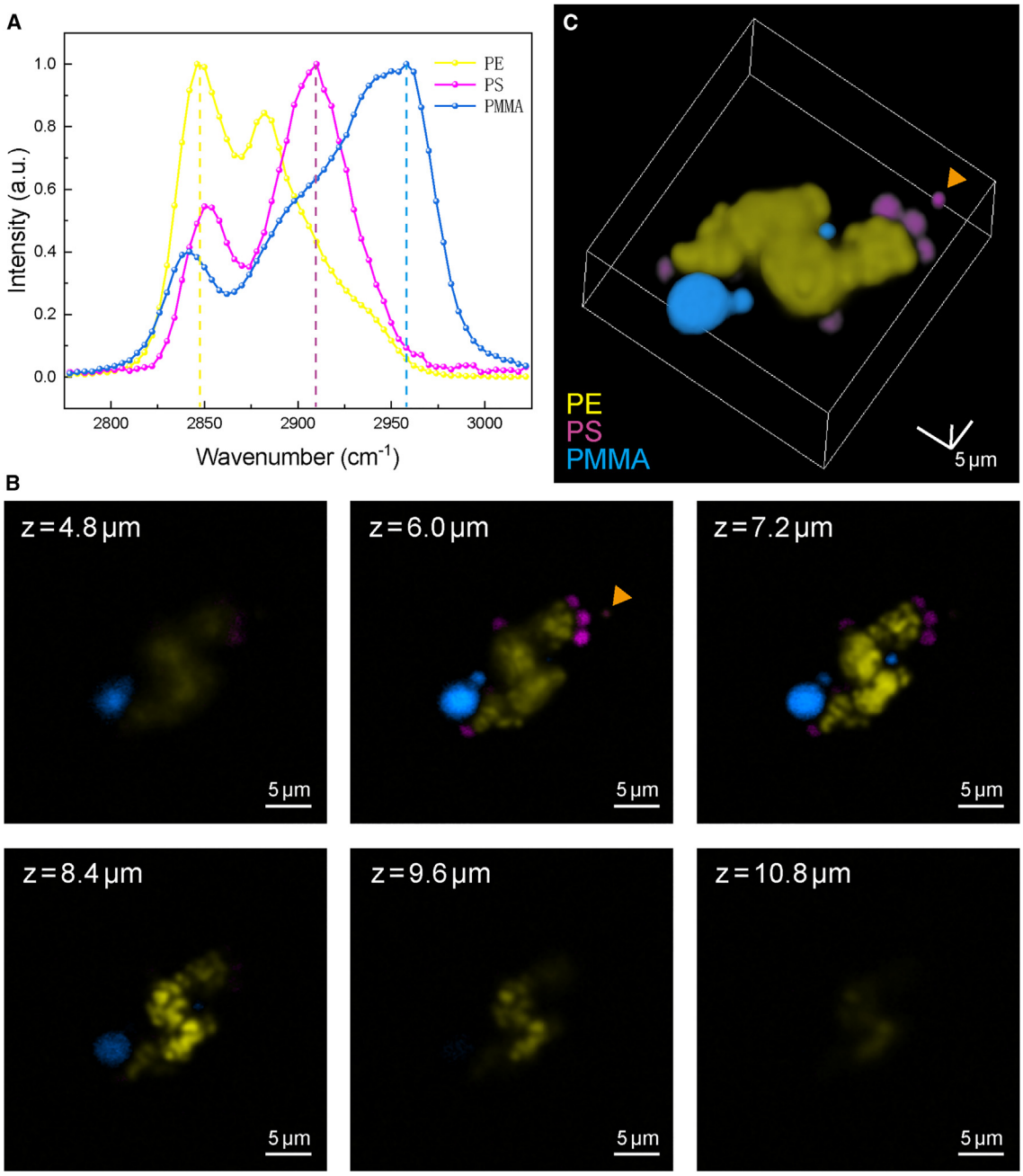

Figure 2. SRS imaging of nano/microplastic mixture

(A) SRS spectra of characteristic peaks of PS, PE, and PMMA.

(B) SRS images of mixed PS, PE, and PMMA mixed samples at different depths in the z axis.

(C) 3D image of mixed PS, PE, and PMMA samples.

Scale bars: 5 μm.

and amorphous powdered polyethylene (PE) were identified. Since most plastics contain a hydrocarbon group (CH_2 and CH_3), it is possible to identify them within a Raman band of 2,750–3,050 cm^{-1} based on their distinct spectral line shapes (Figure 2A). Consequently, the SRS images at 2,910, 2,850, and 2,950 cm^{-1} were used to discriminate between PS, PE, and PMMA with a linear decomposition method (Figure S3).[43] The SRS images of mixed PS, PE, and PMMA samples at different depths in

Please cite this article in press as: Ao et al., Fast detection and 3D imaging of nanoplastics and microplastics by stimulated Raman scattering microscopy, Cell Reports Physical Science (2023), https://doi.org/10.1016/j.xcrp.2023.101623

the z axis are shown in Figure 2B, where yellow represents PE, magenta represents PMMA, and blue represents PS.

3D imaging of nano-/microplastics

The characteristic peaks of PS at 2,910 cm^{-1}, PE at 2,850 cm^{-1}, and PMMA at 2,950 cm^{-1} were selected as the discriminative peaks for SRS imaging. By stepping through the z axis of the samples with a step size of 0.4 μm, we can reconstruct the 3D chemical distribution of the mixed microplastic sample from multiple 2D images that carry different depth information, as shown in Figures 2B and 2C. Among them, the sample surface is set as the zero point in the z direction, and the detection depth is sequentially increased until a complete chemical distribution is obtained.

It can be observed from the 3D imaging results that the three microplastic components can be accurately distinguished at high wavenumbers, and their spatial distribution and 3D topographic features are also clearly identified (Video S1). The PS microspheres are regular spheres with sizes of 2 μm and 500 nm (orange arrowhead), distributed around the PE samples. Most of the PMMA microspheres are in an agglomerated state. From the imaging results at different z positions, the PMMA microspheres with particle sizes of 5 and 2 μm are clearly detected. The PE particles are distributed in irregular aggregates. From the imaging results at different depths, the longitudinal distribution of PE samples is uneven. The depth from z = 7.2 to 8.4 μm is the area where PE is relatively concentrated in the longitudinal direction. As the z value continues to increase, the imaging becomes clearer, and at a depth of Z = 6.0 μm, it is the focal plane of PS and PMMA. From the depth of Z = 4.8 to 6.0 μm, the sharpness of PS and PMMA continues to increase, gradually approaching its true spherical morphology.

Determination of nano-/microplastics in atmospheric environment

In order to verify the ability of SRS for complex environmental samples, we studied the detection of nano-/microplastics in atmospheric environmental samples (Figure 3A). We noticed that few previous works have demonstrated the application of SRS in microplastics detection with sediments and water samples.[39,44] However, the detected Raman bands in these studies were mainly focused on the fingerprint region, sacrificing the identification efficiency with high specificity due to the following reasons. First, the SRS signal generated from fingerprint region was normally lower compared with the high-frequency C-H stretching band, limiting the detection of nano-/microplastics (<5 μm). Second, the Raman peaks of different plastics in the fingerprinting region are quite different, and each peak appeared sharp, which means that a one-shot SRS image could only show one or a few types of microplastics. For the natural environmental samples, the plastics to be determined were unknown and diverse. The detection efficiency would be slowed down by continuous hyper-spectral scanning in each FOV or by adjusting the SRS resonance conditions at multi-characteristic peaks of different plastics. Based on this issue, a detection method in the high-frequency C-H stretching band was proposed here. The on-resonance state of SRS during real-time imaging was focused at 2,865 cm^{-1}, while the off-resonance state was set at 2,810 cm^{-1} (Figure 3B). One-shot SRS images at 2,865 cm^{-1} could reveal numerous kinds of plastics, as a hydrocarbon group was the fundamental composition for most plastics. The spectrum in the fingerprint region of each type of microplastic was collected to prove our judgment (Figure S4), and the results show consistency with the detection method using the high-frequency C-H stretching band. This approach could improve the efficiency of plastics detection in complex environmental samples. However, if the sample contains many organic matters, such as biosamples (like lung tissues demonstrated

Please cite this article in press as: Ao et al., Fast detection and 3D imaging of nanoplastics and microplastics by stimulated Raman scattering microscopy, Cell Reports Physical Science (2023), https://doi.org/10.1016/j.xcrp.2023.101623

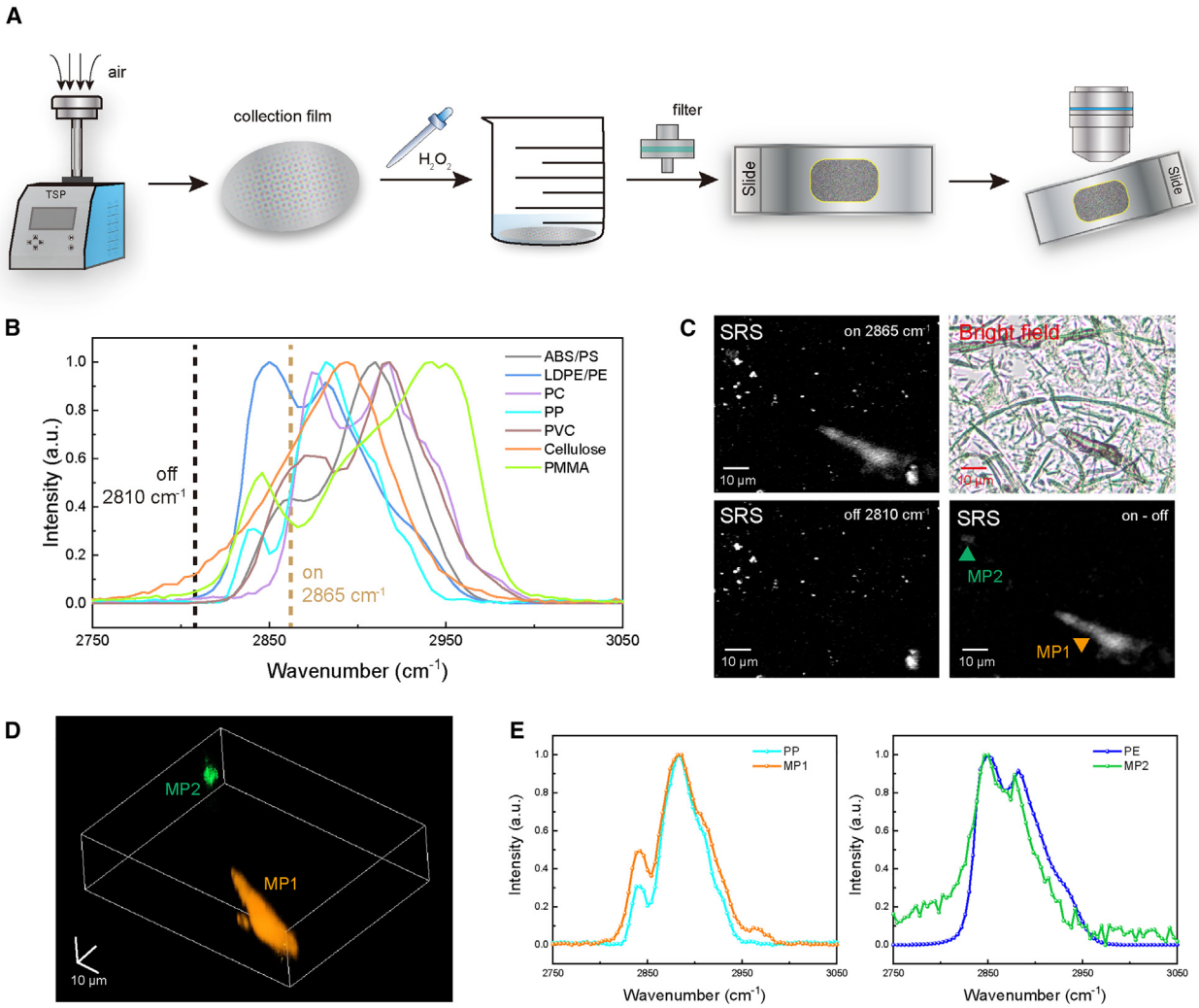

Figure 3. SRS detection of nano-/microplastics in atmospheric samples

(A) Atmospheric sample processing method.

(B) SRS spectra of standard microplastic samples.

(C) SRS imaging of atmospheric sample at different wavenumbers.

(D) 3D image of nano-/microplastics found in atmospheric sample.

(E) SRS spectra of PP (MP1) and PE (MP2) nano-/microplastics found in atmospheric sample.

Scale bars: 10 μm.

below), a digestion treatment (detailed in the supplemental experimental procedures) before testing was necessary to remove the disruption of organic matter. Additionally, the atmospheric environmental samples could also contain many organic substances and other complex components,[45] and these substances may also have characteristic peaks in the high-frequency band, which will interfere with the detection of microplastics.

Figure 3C shows the SRS imaging of preprocessed atmospheric samples. The samples were subjected to the necessary preprocessing steps to remove organic interferences and enhance the quality of the image. It can be observed that under a bright-field optical microscope, there are some interfering substances such as filter debris in the sample, which may become interference in the traditional visual identification method and affect the observation and identification of nano-/microplastics. While SRS imaging can

Please cite this article in press as: Ao et al., Fast detection and 3D imaging of nanoplastics and microplastics by stimulated Raman scattering microscopy, Cell Reports Physical Science (2023), https://doi.org/10.1016/j.xcrp.2023.101623

improve the image contrast, there will be no messy interference such as glass fibers, and the contrast is brighter. In order to ensure that the imaged particles are completely nano-/microplastic particles, the non-resonant wavenumber of 2,810 cm^{-1} is scanned again, and obvious bright-dark changes can be seen in the SRS image. Microplastics do not have a significant peak at 2,810 cm^{-1}, so these residual bright particles at 2,810 cm^{-1} are not microplastics but may be the residual organic components or other impurities that have not been digested. In order to exclude the interference of these substances, we performed subtraction processing on the scanning results at two wavenumbers and subtracted the spectrum at 2,810 cm^{-1} from the spectrum at 2,865 cm^{-1} to obtain the nano-/microplastics in the actual environmental sample, namely particle 1 (MP1) and particle 2 (MP2).

Meanwhile, in order to understand the actual morphology of the two plastics, we carried out 3D imaging analysis, as shown in Figure 3D. The relative position and distribution state of the two microplastics in space were clearly displayed, and the MP1 was larger in size, above 44.1 × 14.8 × 8.9 μm, and showed irregular fragments. The MP2 was smaller in size, about 5.6 × 3.7 × 5.7 μm, and showed an irregular spherical shape, which belonged to particle-type microplastics. For better identification of the type of MP1 and MP2, hyper-spectral scanning was preformed to acquire the SRS spectrum (detailed in the supplemental experimental procedures). Among them, the scanning results of MP1 at high wavenumbers match the characteristic peaks of polypropylene (PP) standard samples (Figure 3E). Through the fingerprint band verification, it is found that the characteristic peaks of low wavenumbers of PP are also consistent (Figure S4). The detected microplastic is thus confirmed as PP, while MP2 has a characteristic peak matching PE in the high-frequency C-H stretching band (Figure 3E), so further verification was carried out at low wavenumbers of 1,100–1,150 cm^{-1}, and it was found that the low wavenumber also completely matched the characteristic peak of PE. This microplastic is thus confirmed as PE.

The atmospheric samples were scanned and analyzed according to the above-established method, and 4 types of nano-/microplastics were detected, including PP, PE, PMMA, and cellulose plastics, and their shapes were granular, fibrous, and fragmented, as shown in Figure 4A. For the microplastics matched to PP and PE in the high wavenumber scan, we carried out low-frequency band detection and verification according to the method described above. For the samples matched as PMMA in the high wavenumber scan, we also selected low wavenumber characteristic peaks of 750–900 and 1,350–1,550 cm^{-1} for verification. For the samples matched to cellulose in the high wavenumber scan, we selected the low wavenumber of 1,000–1,200 cm^{-1} for verification, and the analyte that achieved characteristic peak matching in both high- and low-frequency bands can be confirmed as cellulose plastics. It should be noted that natural fiber cotton (CO) and manmade cellulosic fibers such as viscose (CV) cannot be discriminated with spectroscopic methods. In order to achieve this distinction, microscopic analyses or additional analytical methods as "more lines for evidence" in fiber examinations are recommended.[46] In the atmospheric samples, a total of 38 nano-/microplastics (~9×10^{-4} particles/L) were detected and subjected to analysis for their type and particle size (as shown in Figures 3C, 4A, and S5). Specifically, Figure 4B illustrates the distribution of plastic types identified, while Figure 4C displays the particle size distribution of the detected nano-/microplastics. More than half of the microplastics were identified as PE microplastics, accounting for 55.26%, followed by cellulose microplastics, with a total of 12, accounting for 31.58%. The smaller proportions are PP and PMMA, with only 3 and 2 particles detected, accounting for 7.89% and 5.26%, respectively. Among all the detected microplastics, the number of microplastics with a particle

Please cite this article in press as: Ao et al., Fast detection and 3D imaging of nanoplastics and microplastics by stimulated Raman scattering microscopy, Cell Reports Physical Science (2023), https://doi.org/10.1016/j.xcrp.2023.101623

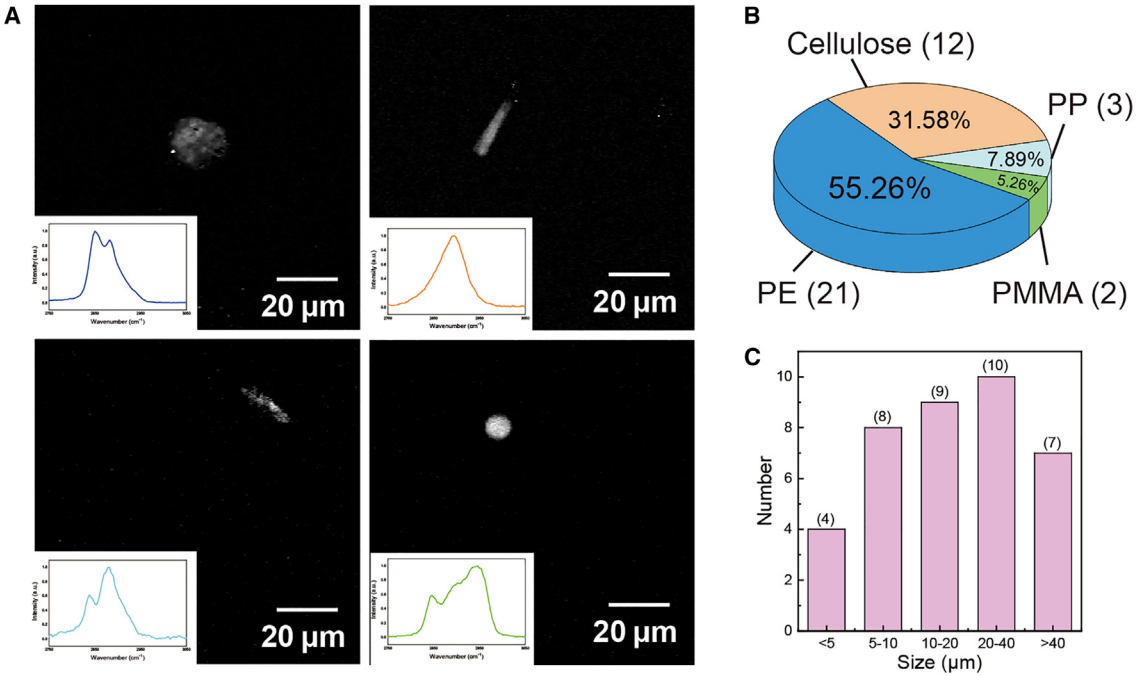

Figure 4. SRS imaging and distribution of nano-/microplastics in atmospheric samples

(A) SRS imaging and spectrum of microplastics in atmospheric samples; (B) Pie chart of the distribution of microplastics in atmospheric samples; (C) Histogram of distribution of nano-/microplastics with different particle sizes in atmospheric samples.

Scale bar: 20 μm.

size below 10 μm accounted for 32%, including 4 tiny nano-/microplastics (<5 μm) detected. The median size distribution of PE particles is less than 20 μm, while cellulose is higher than 40 μm. Although not all PE particles are below 5 μm and all cellulose plastics particles were above 5 μm, t test analysis indicates there is a significant difference between the type and the size of PE and cellulose based on the current data (Figure S6). The SRS analysis results of various nano-/microplastics in atmospheric samples show that the SRS detection method of high wavenumber scanning-low wavenumber verification can be applied to the analysis and identification of various particle sizes and types of microplastics or nanoplastics in the atmospheric environment. This good practice in research on the detection of nano-/microplastics in the atmospheric environment addresses the problem that it is difficult to achieve high spatial resolution and obtain comprehensive morphology characteristics of nano-/microplastics in previous studies. This work provides methodological support for obtaining more accurate and comprehensive 3D information on nano-/microplastics.

Determination of nano-/microplastics in lung tissue

Our detection method has been successfully applied in the microplastic and nanoplastic detection of laboratory standard samples and atmospheric samples. As an additional demonstration, 12 lung tissue samples from hospitals were then analyzed by SRS to study the existence of microplastics or nanoplastics in human lung tissue. Patient demographics, including age and types of lung diseases, are presented in detail in Table S1.

Figures 5A and 5B show the pretreatment procedure of the lung tissues and the SRS detection results of nano-/microplastics in 12 lung tissues. We found the presence of

Please cite this article in press as: Ao et al., Fast detection and 3D imaging of nanoplastics and microplastics by stimulated Raman scattering microscopy, Cell Reports Physical Science (2023), https://doi.org/10.1016/j.xcrp.2023.101623

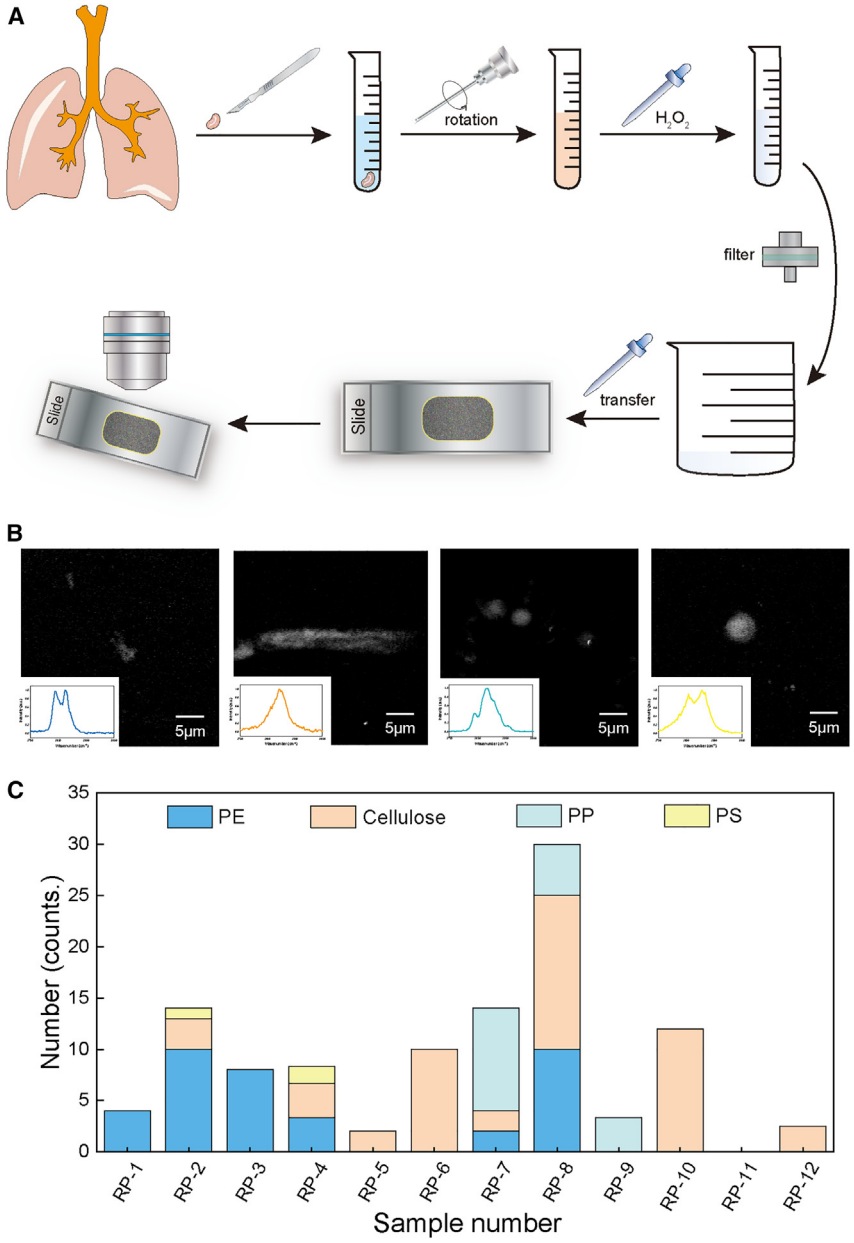

Figure 5. SRS detection of nano-/microplastics in lung tissue

(A) Processing and detection method of lung tissue samples.

(B) SRS spectra and images of microplastics detected in lung tissues.

(C) Distribution of types and quantities of nano-/microplastics in each lung tissue sample.

Scale bars: 5 μm.

nano-/microplastics in 11 lung tissue samples, and a total of 53 nano-/microplastics were detected, including fibrous, fragmented, and granular shapes (see Figure S7 for details of each sample). The 3D structures of microplastics in lung tissues were also recorded (Figure S8). Like the nano-/microplastics detected in atmospheric samples, the tissue samples contain PP, PE, and cellulose nano-/microplastics. The difference is that PS, which is not detected in atmospheric samples, appears in lung tissue, and PMMA, which occurs less frequently in atmospheric samples, is also not detected in lung tissue samples, which may be due to the limited tissue

samples. In order to mitigate the interference caused by tissue volume in quantitative comparisons, we employ normalization by dividing the detected plastic particles by the tissue volume measured using the drainage method (Figure 5C).

Our method was successfully applied to nano-/microplastic detection in human tissue. PP, PE, and PS were detected in human lung tissues, which confirmed the applicability of SRS technology in the detection of microplastics in human tissue, demonstrating its great application potential in related environmental toxicology, air pollution, and human health-related research.

DISCUSSION

The traditional analysis methods of microplastics such as imaging analysis and SEM are limited to the 2D shape of the microplastics. Although the observation of small-sized microplastics can be realized with the help of the high resolution of a SEM instrument, there is a problem of inaccurate characterization and type determination of microplastics.[16,47] Therefore, the morphological characterization of microplastics in previous studies is limited by the constraints of tools and instruments, and it is difficult to achieve a balance between achieving high resolution and obtaining comprehensive morphological features. With the high temporal-spatial resolution, SRS microscopy proved to be a robust method for quantitative and 3D morphology studies of nano-/microplastics through chemical imaging. Specifically, a 512 × 512 pixel SRS image sized as 89.6 × 89.6 μm^2 could be digitized within 1.2 s, whereas MRS takes ~4 h to map a 30 × 30 pixel image with a 15 × 15 μm^2 FOV, achieving ~12,000-fold improvement in frame imaging speed. Meanwhile, SRS offers higher spatial resolution of ~350 nm. By comparison, the resolution of commercial MRS systems is limited around 1 μm. The time required to obtain the 3D structure of particles is indeed influenced by their size. This is because the construction of the 3D structure is based on a series of 2D images acquired along the z axis. Therefore, the total time needed for imaging is estimated by considering the number of image stacks required to cover the entire depth of the particles. For instance, by stepping through the z axis of the samples with a step size of 0.5 μm, a 10 μm plastic particle with one component requires 21 SRS images to render the 3D structure; hence, the acquisition time would be ~25 s. The high resolution of SRS enables small-particle-size and even nanoscale plastics to be efficiently and accurately identified, and its excellent 3D chemical imaging capabilities can also accurately restore the distribution state and morphological characteristics of microplastics in space, which makes the judgment of microplastics morphological types more accurate and provides more comprehensive and reliable supporting information for research on microplastic aging and traceability.

The aim of this work is to offer a methodology of nano-/microplastics detection with SRS imaging. We first verified the capability of SRS in the detection of various types and particle sizes of nano-/microplastics, showing that the current system could achieve single-particle detection even at sizes down to 100 nm. Besides leveraging the advantage of 3D chemical imaging, SRS can obtain the morphology of external mixed microplastic samples. Considering the complexity of natural samples, we further proposed a high wavenumber scanning method accompanied by low wavenumber verification. So as to demonstrate the applicability of this methodological work, we presented two cases of nano-/microplastics detection in atmospheric environmental samples and human lung tissues. Various types of nano-/microplastics such as PP, PE, PMMA, and cellulose plastics were detected in atmospheric environmental samples, and the interference of other impurities was effectively avoided. The 3D morphological characteristics of PP and PE microplastics in the atmosphere

Please cite this article in press as: Ao et al., Fast detection and 3D imaging of nanoplastics and microplastics by stimulated Raman scattering microscopy, Cell Reports Physical Science (2023), https://doi.org/10.1016/j.xcrp.2023.101623

were successfully obtained. Like the nano-/microplastics detected in atmospheric samples, PP, PE, and cellulose nano-/microplastics were detected in 11 of 12 human lung tissue samples, including fibrous, fragmented, and granular shapes.

Some previous studies on microplastics in the atmosphere have shown that PP, PE, and cellulose are the most common types of microplastics in the atmospheric environment.[48–51] The size of atmospheric microplastics in previous studies was mainly restricted by the sampling method and the level of detection and analysis, usually concentrated in a few hundred microns, while most of the microplastics in this study are below tens of microns, and only a few particles can reach nearly a hundred microns. Since the particle size of atmospheric particles is closely related to whether they can enter the human body through the respiratory system and other metabolic pathways, the size of microplastics needs to be paid attention to in atmospheric microplastic research. High concentrations of air pollutants may induce chronic inflammatory responses in the respiratory tract, which are associated with cardiovascular and respiratory diseases.[52] Based on this study, more attention should be paid to the result that atmospheric microplastics are more concentrated in small-size particles and long fibers. In future research, SRS technology is expected to play an important role in the morphology characterization, detection, and analysis of small-sized microplastics in the environment, as well as in toxicological studies on air pollution and human health, providing solid methodological support.

A recent study by Amato-Lourenço et al. demonstrated the presence of microplastics in lung tissue, with PP and PE being the most common types,[53] which shows similar results to our findings. Although our study showed a higher microplastics detection rate in lung tissue, the comparison is not simple due to different experimental apparatuses and lung tissue sample processing methods. For example, in the study of Amato-Lourenço, lung tissue samples were digested at 60°C by mixing digestive enzymes for 12 h, density separated with $ZnCl_2$, and filtered onto a silver membrane for Raman testing, which was achieved by a 633 nm laser. In addition, the selection of patients in previous studies included death due to hypovolemic shock and abdominal hemorrhage and patients with cerebral infarction, who may be less exposed to polluted air than those with lung disease. The difference of detecting instruments would also affect the results. The deposition of exogenous particulate matter in the lung includes three basic mechanisms, inertial collision, deposition, and diffusion, and is affected by many factors such as shape, particle size, and density. Some studies show that particles smaller than 3 μm are more likely to enter the deep location of lung tissues.[54] Among the microplastics detected in lung tissue samples by SRS in this study, most of the particles were between 1 and 2 μm, and the fibrous microplastics were longer in length, but their physical diameters were also below 3 μm. It is also worth noting that some of the particles are nanoplastics (Figure S7, arrows).

The results of our analysis agree with the idea that the respiratory system is indeed an important pathway for human microplastic exposure and that microplastic accumulation does exist in lung tissue. However, more robust studies are needed to prove the relationship between the presence of microplastics in lung tissue and lung disease and human health. Although microplastics are one of the important air pollutants, current research does not have direct and sufficient evidence to prove that microplastics are directly related to the above-mentioned diseases. The current work focuses on the methodology, providing a strategy for rapid screening of microplastic particles in natural samples and for revealing the existence of microplastics in lung tissue samples, and we expect it to aid future robust testing to help develop correlations between accumulation and health.

There are still some deficiencies in the application of SRS in the field of nano-/microplastics detection research. For example, one-shot SRS images only presented a specific resonance Raman peak, lacking the full spectral information. To verify the types of plastics, standard spontaneous Raman spectra as a benchmark are a prerequisite. In addition, dyes might contribute huge transient absorption background and so overwhlem the resolvable SRS signal. The above problems make it difficult to establish a comprehensive and complete SRS microplastics standard database, which has an impact on the quantitative research of nano-/microplastics. Future research is needed to better apply SRS toward the accurate, comprehensive, and rapid detection and characterization of nano-/microplastics.

EXPERIMENTAL PROCEDURES

Resource availability

Lead contact

Further information and requests for resources should be directed to the corresponding author, Liwu Zhang (zhanglw@fudan.edu.cn).

Materials availability

This study did not generate new unique reagents.

Data and code availability

All study data are included in the article and the supplemental information.

SUPPLEMENTAL INFORMATION

Supplemental information can be found online at https://doi.org/10.1016/j.xcrp.2023.101623.

ACKNOWLEDGMENTS

The authors gratefully acknowledge financial support from the National Natural Science Foundation of China (nos. 22176036, 21976030, and 22006020) and the Natural Science Foundation of Shanghai (no. 19ZR1471200).

AUTHOR CONTRIBUTIONS

L.Z. and M.J. supervised the project and led the overall effort. J.A. and G.X. designed the experiments. L.Z. and M.J. revised the manuscript. H.W. and T.C. collected the human lung tissues. G.X. and L.X. pretreated the experimental samples and carried out the MRS measurements. J.A. drew the illustrations and carried out the SRS measurements. J.L., K.G., X.R., J.H., K.L., and W.W. assisted with data collection and analysis. The manuscript was written by G.X., J.A., and L.X., with all authors' efforts.

DECLARATION OF INTERESTS

The authors declare no competing interests.

INCLUSION AND DIVERSITY

We support inclusive, diverse, and equitable conduct of research.

Received: April 23, 2023
Revised: July 27, 2023
Accepted: September 13, 2023
Published: October 9, 2023

REFERENCES

1. Andrady, A.L. (2011). Microplastics in the marine environment. Mar. Pollut. Bull. *62*, 1596–1605.
2. Dris, R., Imhof, H., Sanchez, W., Gasperi, J., Galgani, F., Tassin, B., and Laforsch, C. (2015). Beyond the ocean: contamination of freshwater ecosystems with (micro-)plastic particles. Environ. Chem. *12*, 539.
3. Wagner, S., and Reemtsma, T. (2019). Things we know and don't know about nanoplastic in the environment. Nat. Nanotechnol. *14*, 300–301.
4. Rodrigues, M.O., Abrantes, N., Gonçalves, F.J.M., Nogueira, H., Marques, J.C., and Gonçalves, A.M.M. (2019). Impacts of plastic products used in daily life on the environment and human health: What is known? Environ. Toxicol. Pharmacol. *72*, 103239.
5. Ma, Y., Huang, A., Cao, S., Sun, F., Wang, L., Guo, H., and Ji, R. (2016). Effects of nanoplastics and microplastics on toxicity, bioaccumulation, and environmental fate of phenanthrene in fresh water. Environ. Pollut. *219*, 166–173.
6. Triebskorn, R., Braunbeck, T., Grummt, T., Hanslik, L., Huppertsberg, S., Jekel, M., Knepper, T.P., Krais, S., Müller, Y.K., Pittroff, M., et al. (2019). Relevance of nano- and microplastics for freshwater ecosystems: A critical review. TrAC-Trends Anal. Chem. *110*, 375–392.
7. Vethaak, A.D., and Leslie, H.A. (2016). Plastic Debris Is a Human Health Issue. Environ. Sci. Technol. *50*, 6825–6826.
8. Li, D., Shi, Y., Yang, L., Xiao, L., Kehoe, D.K., Gun'ko, Y.K., Boland, J.J., and Wang, J.J. (2020). Microplastic release from the degradation of polypropylene feeding bottles during infant formula preparation. Nat. Food *1*, 746–754.
9. Hernandez, L.M., Xu, E.G., Larsson, H.C.E., Tahara, R., Maisuria, V.B., and Tufenkji, N. (2019). Plastic Teabags Release Billions of Microparticles and Nanoparticles into Tea. Environ. Sci. Technol. *53*, 12300–12310.
10. Hernandez, L.M., Xu, E.G., Larsson, H.C.E., Tahara, R., Maisuria, V.B., and Tufenkji, N. (2020). Response to Comment on "Plastic Teabags Release Billions of Microparticles and Nanoparticles into Tea". Environ. Sci. Technol. *54*, 14136–14137.
11. Busse, K., Ebner, I., Humpf, H.-U., Ivleva, N., Kaeppler, A., Oßmann, B.E., and Schymanski, D. (2020). Comment on "Plastic Teabags Release Billions of Microparticles and Nanoparticles into Tea". Environ. Sci. Technol. *54*, 14134–14135.
12. Zhou, X.X., He, S., Gao, Y., Chi, H.Y., Wang, D.J., Li, Z.C., and Yan, B. (2021). Quantitative Analysis of Polystyrene and Poly(methyl methacrylate) Nanoplastics in Tissues of Aquatic Animals. Environ. Sci. Technol. *55*, 3032–3040.
13. Zhang, Q., Xu, E.G., Li, J., Chen, Q., Ma, L., Zeng, E.Y., and Shi, H. (2020). A Review of Microplastics in Table Salt, Drinking Water, and Air: Direct Human Exposure. Environ. Sci. Technol. *54*, 3740–3751.
14. Ragusa, A., Svelato, A., Santacroce, C., Catalano, P., Notarstefano, V., Carnevali, O., Papa, F., Rongioletti, M.C.A., Baiocco, F., Draghi, S., et al. (2021). Plasticenta: First evidence of microplastics in human placenta. Environ. Int. *146*, 106274.
15. Schwabl, P., Köppel, S., Königshofer, P., Bucsics, T., Trauner, M., Reiberger, T., and Liebmann, B. (2019). Detection of Various Microplastics in Human Stool: A Prospective Case Series. Ann. Intern. Med. *171*, 453–457.
16. Dehghani, S., Moore, F., and Akhbarizadeh, R. (2017). Microplastic pollution in deposited urban dust, Tehran metropolis, Iran. Environ. Sci. Pollut. Res. Int. *24*, 20360–20371.
17. Shim, W.J., Hong, S.H., and Eo, S.E. (2017). Identification methods in microplastic analysis: a review. Anal. Methods *9*, 1384–1391.
18. Liu, K., Wang, X., Wei, N., Song, Z., and Li, D. (2019). Accurate quantification and transport estimation of suspended atmospheric microplastics in megacities: Implications for human health. Environ. Int. *132*, 105127.
19. Cai, L., Wang, J., Peng, J., Tan, Z., Zhan, Z., Tan, X., and Chen, Q. (2017). Characteristic of microplastics in the atmospheric fallout from Dongguan city, China: preliminary research and first evidence. Environ. Sci. Pollut. Res. Int. *24*, 24928–24935.
20. Zhang, W., Dong, Z., Zhu, L., Hou, Y., and Qiu, Y. (2020). Direct Observation of the Release of Nanoplastics from Commercially Recycled Plastics with Correlative Raman Imaging and Scanning Electron Microscopy. ACS Nano *14*, 7920–7926.
21. Xu, G., Cheng, H., Jones, R., Feng, Y., Gong, K., Li, K., Fang, X., Tahir, M.A., Valev, V.K., and Zhang, L. (2020). Surface-Enhanced Raman Spectroscopy Facilitates the Detection of Microplastics <1 mum in the Environment. Environ. Sci. Technol. *54*, 15594–15603.
22. Peng, C., Tang, X., Gong, X., Dai, Y., Sun, H., and Wang, L. (2020). Development and Application of a Mass Spectrometry Method for Quantifying Nylon Microplastics in Environment. Anal. Chem. *92*, 13930–13935.
23. Xu, G., Cheng, H., Jones, R., Feng, Y., Gong, K., Li, K., Fang, X., Tahir, M.A., Valev, V.K., and Zhang, L. (2020). Surface-Enhanced Raman Spectroscopy Facilitates the Detection of Microplastics <1 μm in the Environment. Environ. Sci. Technol. *54*, 15594–15603.
24. Freudiger, C.W., Min, W., Saar, B.G., Lu, S., Holtom, G.R., He, C., Tsai, J.C., Kang, J.X., and Xie, X.S. (2008). Label-free biomedical imaging with high sensitivity by stimulated Raman scattering microscopy. Science *322*, 1857–1861.
25. Nandakumar, P., Kovalev, A., and Volkmer, A. (2009). Vibrational imaging based on stimulated Raman scattering microscopy. New J. Phys. *11*, 033026.
26. Ozeki, Y., Dake, F., Kajiyama, S., Fukui, K., and Itoh, K. (2009). Analysis and experimental assessment of the sensitivity of stimulated Raman scattering microscopy. Opt Express *17*, 3651–3658.
27. Saar, B.G., Freudiger, C.W., Reichman, J., Stanley, C.M., Holtom, G.R., and Xie, X.S. (2010). Video-rate molecular imaging in vivo with stimulated Raman scattering. Science *330*, 1368–1370.
28. Cheng, J.X., and Xie, X.S. (2015). Vibrational spectroscopic imaging of living systems: An emerging platform for biology and medicine. Science *350*, aaa8870.
29. Hu, F., Shi, L., and Min, W. (2019). Biological imaging of chemical bonds by stimulated Raman scattering microscopy. Nat. Methods *16*, 830–842.
30. Cheng, Q., Wei, L., Liu, Z., Ni, N., Sang, Z., Zhu, B., Xu, W., Chen, M., Miao, Y., Chen, L.Q., et al. (2018). Operando and three-dimensional visualization of anion depletion and lithium growth by stimulated Raman scattering microscopy. Nat. Commun. *9*, 2942.
31. Ling, J., Miao, X., Sun, Y., Feng, Y., Zhang, L., Sun, Z., and Ji, M. (2019). Vibrational Imaging and Quantification of Two-Dimensional Hexagonal Boron Nitride with Stimulated Raman Scattering. ACS Nano *13*, 14033–14040.
32. Ao, J., Feng, Y., Wu, S., Wang, T., Ling, J., Zhang, L., and Ji, M. (2020). Rapid, 3D Chemical Profiling of Individual Atmospheric Aerosols with Stimulated Raman Scattering Microscopy. Small Methods *4*.
33. Bae, K., Zheng, W., Ma, Y., and Huang, Z. (2020). Real-Time Monitoring of Pharmacokinetics of Mitochondria-Targeting Molecules in Live Cells with Bioorthogonal Hyperspectral Stimulated Raman Scattering Microscopy. Anal. Chem. *92*, 740–748.
34. Cheng, Q., Miao, Y., Wild, J., Min, W., and Yang, Y. (2021). Emerging applications of stimulated Raman scattering microscopy in materials science. Matter *4*, 1460–1483.
35. Gong, K., Ao, J., Li, K., Liu, L., Liu, Y., Xu, G., Wang, T., Cheng, H., Wang, Z., et al. (2023). Imaging of pH distribution inside individual microdroplet by stimulated Raman microscopy. Proc. Natl. Acad. Sci. *120*, e2219588120.
36. Li, H., Cheng, Y., Tang, H., Bi, Y., Chen, Y., Yang, G., Guo, S., Tian, S., Liao, J., Lv, X., et al. (2020). Imaging Chemical Kinetics of Radical Polymerization with an Ultrafast Coherent Raman Microscope. Adv. Sci. *7*, 1903644.
37. Liao, C.-S., Wang, P., Huang, C.Y., Lin, P., Eakins, G., Bentley, R.T., Liang, R., and Cheng, J.-X. (2018). In Vivo and in Situ Spectroscopic Imaging by a Handheld Stimulated Raman Scattering Microscope. ACS Photonics *5*, 947–954.
38. Zhang, C., Huang, K.-C., Rajwa, B., Li, J., Yang, S., Lin, H., Liao, C.-s., Eakins, G., Kuang, S., Patsekin, V., et al. (2017). Stimulated Raman scattering flow cytometry for label-free single-particle analysis. Optica *4*, 103–109.
39. Zada, L., Leslie, H.A., Vethaak, A.D., Tinnevelt, G.H., Jansen, J.J., de Boer, J.F., and Ariese, F. (2018). Fast microplastics identification with

stimulated Raman scattering microscopy. J. Raman Spectrosc. *49*, 1136–1144.

40. Genchi, L., Martin, C., Laptenok, S.P., Baalkhuyur, F., Duarte, C.M., and Liberale, C. (2023). When microplastics are not plastic: Chemical characterization of environmental microfibers using stimulated Raman microspectroscopy. Sci. Total Environ. *892*, 164671.

41. Laptenok, S.P., Martin, C., Genchi, L., Duarte, C.M., and Liberale, C. (2020). Stimulated Raman microspectroscopy as a new method to classify microfibers from environmental samples. Environ. Pollut. *267*, 115640.

42. Bi, Y., Yang, C., Chen, Y., Yan, S., Yang, G., Wu, Y., Zhang, G., and Wang, P. (2018). Near-resonance enhanced label-free stimulated Raman scattering microscopy with spatial resolution near 130 nm. Light Sci. Appl. *7*, 81.

43. Ji, M., Orringer, D.A., Freudiger, C.W., Ramkissoon, S., Liu, X., Lau, D., Golby, A.J., Norton, I., Hayashi, M., Agar, N.Y.R., et al. (2013). Rapid, label-free detection of brain tumors with stimulated Raman scattering microscopy. Sci. Transl. Med. *5*, 201ra119.

44. Laptenok, S.P., Martin, C., Genchi, L., Duarte, C.M., and Liberale, C. (2020). Stimulated Raman microspectroscopy as a new method to classify microfibers from environmental samples. Environ. Pollut. *267*, 115640.

45. Ao, J., Feng, Y., Wu, S., Wang, T., Ling, J., Zhang, L., and Ji, M. (2020). Rapid, 3D Chemical Profiling of Individual Atmospheric Aerosols with Stimulated Raman Scattering Microscopy. Small Methods *4*.

46. Stark, M. (2022). Plausibility Checks Are Needed in Microplastic Research to Prevent Misinterpretations. Environ. Sci. Technol. *56*, 17495–17497.

47. Courtene-Jones, W., Quinn, B., Gary, S.F., Mogg, A.O.M., and Narayanaswamy, B.E. (2017). Microplastic pollution identified in deep-sea water and ingested by benthic invertebrates in the Rockall Trough, North Atlantic Ocean. Environ. Pollut. *231*, 271–280.

48. Cai, L., Wang, J., Peng, J., Tan, Z., Zhan, Z., Tan, X., and Chen, Q. (2017). Characteristic of microplastics in the atmospheric fallout from Dongguan city, China: preliminary research and first evidence. Environ. Sci. Pollut. Res. Int. *24*, 24928–24935.

49. Dris, R., Gasperi, J., Saad, M., Mirande, C., and Tassin, B. (2016). Synthetic fibers in atmospheric fallout: A source of microplastics in the environment? Mar. Pollut. Bull. *104*, 290–293.

50. Caracci, E., Vega-Herrera, A., Dachs, J., Berrojalbiz, N., Buonanno, G., Abad, E., Llorca, M., Moreno, T., and Farré, M. (2023). Micro(nano)plastics in the atmosphere of the Atlantic Ocean. J. Hazard Mater. *450*, 131036.

51. O'Brien, S., Rauert, C., Ribeiro, F., Okoffo, E.D., Burrows, S.D., O'Brien, J.W., Wang, X., Wright, S.L., and Thomas, K.V. (2023). There's something in the air: A review of sources, prevalence and behaviour of microplastics in the atmosphere. Sci. Total Environ. *874*, 162193.

52. Gillibert, R., Balakrishnan, G., Deshoules, Q., Tardivel, M., Magazzù, A., Donato, M.G., Maragò, O.M., Lamy de La Chapelle, M., Colas, F., Lagarde, F., and Gucciardi, P.G. (2019). Raman Tweezers for Small Microplastics and Nanoplastics Identification in Seawater. Environ. Sci. Technol. *53*, 9003–9013.

53. Amato-Lourenço, L.F., Carvalho-Oliveira, R., Júnior, G.R., Dos Santos Galvão, L., Ando, R.A., and Mauad, T. (2021). Presence of airborne microplastics in human lung tissue. J. Hazard Mater. *416*, 126124.

54. Tetley, T.D. (1993). New perspectives on basic mechanisms in lung disease. 6. Proteinase imbalance: its role in lung disease. Thorax *48*, 560–565.